because the output decade replaces the contents of the central decade in the delay units. After this replacement has been accomplished the contents in the delay units are shifted one bit and the testing of the new central decade takes place. The whole process contains the following three conditionally related processing steps:

Step 1: The decade of delta samples under test (central decade) is compared to a set of most probable decades which have been stored in an LUT (LUT 1). If the present decade is the same with one in the set, the decade is not altered and filtering process continues to the next decade, otherwise step 2 follows.

Step 2: The sums of the three decades (summation of their bits) together with the endpoint bits of the central decade are used as an entry to a second LUT (LUT2). If such a combination is valid as an entry to this LUT, the content of the central decade is changed according to the information stored in the LUT and the processing of the next decade follows, otherwise step 3 follows.

Step 3: Here only the sum of the central decade bits and its endpoint bits are used as data entry to a third LUT (LUT 3). If this data entry is valid, the decade is replaced by the one in this LUT, otherwise the decade remains unchanged and the filtering process continues with the next one.

Simulation results: The proposed nonlinear filtering technique has been developed as a simulation package running on a personal computer (IBM PC or compatible). The response of the recursive (Fig. 1) to pure sinusoids was tested first. It was found that there was no degradation in the signal, and the error (MSE), which is generated in the filtering process, was significantly smaller than the quantisation error in the input DM signal. A simulated noisy signal was then filtered. The noise embedded in the signal was of the kind modelled at the beginning of this Letter. The time interval between two consecutive spikes has an average length of 20 DM samples. This time period is larger than the window length (a decade of DM samples). The average power of each spike is about $80\Delta^2$ ($\Delta = 10\,V/256 = 0{\cdot}04\,V$) depending on the slope and the amplitude of the signal. Its width t_w in this case was selected to be eight DM samples (smaller than the decade). The noisy signal $y(n)$ is depicted in Fig. 2(ii). It means square error compared to the original DM signal $x(n)$ (Fig. 2(i)) was found to be $4\Delta^2$ ($6{\cdot}376 \times 10^{-3}\,V^2$). After filtering the new DM signal $z(n)$ (Fig. 2(iii)) was found to have an MSE compared to the original signal $x(n)$ of $1{\cdot}4\Delta^2$ ($2{\cdot}275 \times 10^{-3}\,V$). The power of the noise was reduced almost to a third of its original value. It was also found using various noise specifications that the proposed algorithm performs better when the time interval between noisy spikes is greater than a decade of samples and the spike width is smaller than this time length. This is similar to the behaviour of median filters when they are used to filter out salt and pepper noise.[4] The performance of the nonlinear DM filter degrades when the frequency of the signal increases in accordance with the behaviour of median filters which perform best with constant valued signals. Finally, as with recursive median filters, the output is a root signal, i.e. no improvement in the MSE is observed when the same recursive nonlinear algorithm is used again. The algorithm is not computationally complex although it contains three conditionally dependent processing steps. Actually only the contents of the LUTs have to be defined for a different window length. The general structure of Fig. 1 remains unchanged.

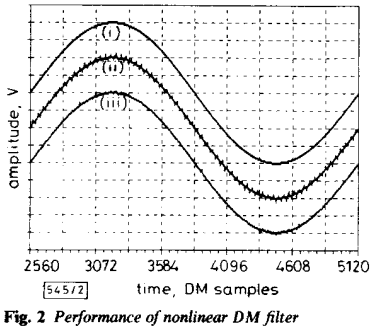

Fig. 2 *Performance of nonlinear DM filter*
a Original DM signal $x(n)$
b Noisy DM signal $y(n)$
c Filtered output $z(n)$ using recursive structure

With a slight modification to the algorithm a nonrecursive implementation can also be obtained using the architecture of Fig. 1. However, to achieve the same filtering performance as with the recursive filter it requires six or seven passes of the signal through the nonrecursive structure.

In conclusion the proposed nonlinear DM filter sufficiently suppresses spiky noise with a behaviour similar to that of median filters. Work continues along these lines to determine proper choice of window length, with respect to the distribution of the time intervals between noisy spikes, spike power etc.

S. L. HORIANOPOULOS
V. ANASTASSOPOULOS
T. DELIYANNIS

Electronics Laboratory
University of Patras
261 10, Patras, Greece

8th April 1991

References

1 ANASTASSOPOULOS, V., KOUVARAS, N., and DELIYANNIS, T.: 'Method for designing half-band delta-modulation FIR filters', *IEE Proc. F*, 1985, **132**, pp. 13–17
2 ANASTASSOPOULOS, V., and DELIYANNIS, T.: 'Efficient implementation of N-th band FIR filters based on a simple window method', *IEE Proc. G*, 1990, **137**, pp. 302–308
3 KOUVARAS, N.: 'Operation of delta modulated signals and their application in the realization of digital filters', *Radio and Electron. Eng.*, 1978, **48**, pp. 431–438
4 GALLAGHER, N. C., and WISE, G. L.: 'A theoretical analysis of the properties of median filters', *IEEE Trans.*, December 1981, **ASSP-39**, pp. 1136–1141

ENHANCED OXYGEN PLASMA STRIPPING OF P^+-IMPLANTED NEGATIVE RESIST BY HYDROGEN PLASMA PRETREATMENT: TEMPERATURE EFFECTS

Indexing terms: Ion implantation, Plasmas

Hydrogen plasma pretreatment (90–115°C, 10–30 min) of P^+-implanted (100 keV, 1×10^{15} ion/cm^2) HR-200 negative resist greatly reduces its resistance to oxygen plasma stripping at about 40°C. At lower temperature for hydrogen plasma pretreatment (down to 40°C) and higher temperature for oxygen plasma stripping (up to 115°C), the reduction to resistance of oxygen plasma stripping by hydrogen plasma pretreatment is much smaller.

Introduction: Reports have been made on the fact that exposure of positive resists doped with ions such as silicon, aluminium, bismuth, phosphorus, arsenic, boron and other metal ions to hydrogen reactive ion etching (RIE) reduces the resistance of these resists to oxygen plasma ashing.[1,2] The hydrogen RIE causes the formation of hydrides of these ions which are volatile at room temperature resulting in easier and faster oxygen plasma ashing. However, the temperature effects of hydrogen and oxygen plasmas to the stripping (etching, ashing) of ion-implanted negative resist have not yet been thoroughly studied. We report the temperature effects of hydrogen plasma pretreatment and oxygen plasma stripping on the P^+-implanted negative resist HR-200.

Experimental: The plasma etching apparatus used was a parallel plate electrode reactor system (Samco basic plasma kit BP-1). The samples were placed on a grounded lower electrode which was connected to a substrate temperature controller. The grounded lower electrode was 2·5 cm away from the powered upper electrode (13·56 MHz). Both electrodes were stainless steel round plates with a diameter of 8 cm. Hydrogen (99·995%) and oxygen (99·995%) were obtained from Air-liquid. The conditions of hydrogen plasma pretreatment were 100 W, 20 sccm and 0·2 torr. The conditions of oxygen plasma stripping were 100 W, 40 sccm and 0·45 torr. The negative resist used for this study was Hunt HR-200 with a thickness of 1·1 μm spin coated on Si wafers. The doping of 1×10^{15} ion/cm^2 for both B^+ and P^+ to HR-200 on Si wafer was performed by a Varian Extrion 200-20A ion implantation system at 100 keV. The remaining thickness after oxygen plasma stripping was measured using a Dektak 3030 stylus surface profilometer.

Results and discussion: The remaining thickness of undoped HR-200, B^+ doped HR-200 (B^+/HR-200) and P^+ doped HR-200 (P^+/HR-200) after oxygen plasma stripping (40°C, 20 minutes) as a function of hydrogen plasma pretreatment time (0–30 minutes) at 90°C is shown in Fig. 1. Only the resistance to oxygen plasma stripping of P^+-implanted (doped) HR-200 was greatly reduced at the conditions in this study. Fig. 2 shows that the plots of remaining thickness of HR-200, B^+/HR-200 and P^+/HR-200 with hydrogen plasma pretreatment

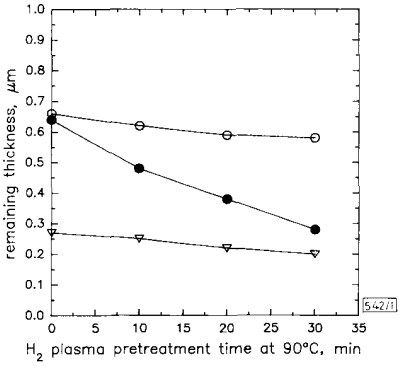

Fig. 1 *Plots of remaining thickness of HR-200, B^+/HR-200, and P^+/HR-200 after oxygen plasma stripping (40°C, 20 minutes) against hydrogen plasma pretreatment time at 90°C*

○ B^+/HR-200
● P^+/HR-200
▽ HR-200
Original thickness = 1·1 μm

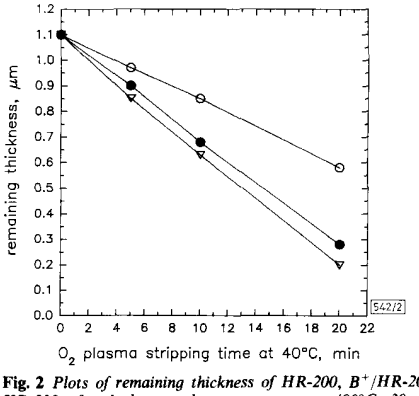

Fig. 2 *Plots of remaining thickness of HR-200, B^+/HR-200, and P^+/HR-200 after hydrogen plasma pretreatment (90°C, 30 min) against oxygen plasma stripping time at 40°C*

○ B^+/HR-200
● P^+/HR-200
▽ HR-200

(90°C, 30 min) against oxygen plasma stripping time (0–20 min) at 40°C are linear. This linearity indicates that they have equal stripping rates at the conditions of this oxygen plasma. Because P^+/HR-200 shows the greatest reduction to oxygen plasma stripping by hydrogen plasma pretreatment in this study, further work focuses temperature effects on P^+/HR-200 only. The temperature effect (40–115°C) of hydrogen plasma pretreatment on the oxygen plasma stripping rate of P^+/HR-200 is shown in Fig. 3. The stripping rate of P^+/HR-200 is linearly correlated with increasing hydrogen plasma pretreatment temperature. The dependence of ln P^+/HR-200 stripping rates on oxygen plasma stripping temperature without and with hydrogen plasma pretreatment at various temperature is shown in Fig. 4. Again, a linear relationship is

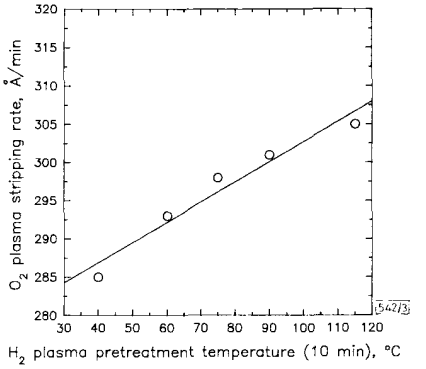

Fig. 3 *Stripping rate of P^+/HR-200 by oxygen plasma stripping (40°C, 10 min) as function of hydrogen plasma pretreatment temperature (10 min)*

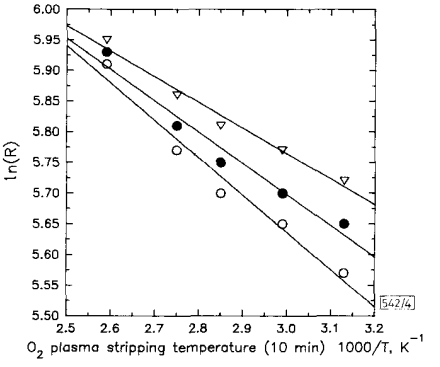

Fig. 4 *Dependence of oxygen plasma stripping rate of P^+/HR-200 on oxygen plasma stripping temperature (10 min) without and with hydrogen plasma pretreatment (10 min) at 40 and 115°C*

R = O_2 plasma stripping rate, Å/min
○ without H_2 plasma pretreatment
E_{act} = 1·263 kcal/mole
● H_2 plasma pretreatment
40°C, 10 min
E_{act} = 1·263 kcal/mole
▽ H_2 plasma pretreatment
115°C, 10 min
E_{act} = 0·854 kcal/mole

found. The activation energies E_{act} are obtained from a linear regression fit of data in Fig. 4 to the standard Arrhenius expression.[3] The energy of activation of P^+/HR-200 was brought down from 1·263 to 0·854 kcal/mole with hydrogen plasma pretreatment at 115°C for 10 min. At lower temperatures for hydrogen plasma pretreatment (down to 40°C) and higher temperatures for oxygen plasma stripping (up to 115°C), the reduction of resistance of oxygen plasma stripping with hydrogen plasma pretreatment is much smaller. Temperatures higher than 115°C have not been tested because HR-200 itself will be softened and thermally decomposed under such temperatures.

Conclusions: The temperature effects of hydrogen plasma preatreatment and low power oxygen plasma stripping on P^+-implanted negative resist HR-200 have been studied. The energy of activation of P^+-implanted negative resist HR-200 by oxygen plasma stripping can be decreased with the hydrogen plasma pretreatment.

W.-A. LOONG
M.-S. YEN

Institute of Applied Chemistry
National Chiao Tung University
Hsinchu, Taiwan 30050, Republic of China

8th April 1991

References

1 HIRAOKA, H.: 'Selective removal of metal atoms in hydrogen reactive ion etching', *J. Vac. Sci. Technol.*, 1986, **B4**, (1), pp. 345–348
2 FUJIMURA, S., KONNO, J., HIKAZUTANI, K., and YANO, H.: 'Ashing of ion-implanted resist layer', *Jpn. J. Appl. Phys.*, 1989, **28**, (10), pp. 2130–2136
3 LOEWENSTEIN, L. M., HUFFMAN, C. H., and DAVIS, C. J.: 'Photoresist stripping using a remote plasma: chemical and transport effects'. Mat. Res. Soc. Symp. Proc., 1987, **98**, pp. 267–272

MODIFIED MULTIQUANTUM BARRIER FOR 600 nm RANGE AlGaInP LASERS

Indexing terms: Semiconductor lasers, Lasers

A new multiquantum barrier (MQB) to obtain a large potential cladding for visible AlGaInP lasers is proposed. The effective potential barrier enhanced by the MQB concept can be increased by constructing the MQB well layer with a smaller energy gap material rather than that of the active layer. Even for 600 nm range lasers, the actual potential barrier height which electrons in the active layer feel under biased condition can be bigger than 200 meV.

A multiquantum barrier (MQB)[1,2] was proposed to enhance carrier confinement of DH structure lasers by virtually increasing the potential barrier using the interference of the reflected electron wave from each boundary of superlattices. In our previous study,[3] we optimised the MQB structure by examining possible choices of well and barrier thicknesses and pair number for a visible AlGaInP laser in the 630 nm wavelength range. We confirmed that an effective potential barrier can be twice as high as a classical potential barrier U_0 by introducing the MQB. However, in that MQB structure, there was a limitation in effective potential barrier height when the Al fraction was increased in the active layer. Therefore, it has been difficult to obtain a sufficient barrier height for 600 nm range lasers even by using the MQB. We propose a modified MQB structure and show that this MQB is useful for wavelength shortening of AlGaInP visible lasers.

Fig. 1 shows the potential profile of an original MQB (*a*) and the modified MQB (*b*). To obtain a larger energy gap difference between well and barrier at the MQB region and to increase effective potential barrier, we have constructed the well layer with smaller energy gap material rather than that of the active layer material. That is, we have chosen the well layer Al fraction x_w as following the relation $x_w < x_a < x_b$, where x_a and x_b are the Al fraction of the active and the MQB barrier layers, respectively. In such a case, we have to carefully choose the well thickness so as not to cause absorption of emitted light at the MQB region. Fig. 2 shows the quantised energy gap calculated in a simple square well model as a function of well width with varying Al composition of the well layer. In the proper procedure, we must calculate the quantised energy level as a miniband, but in an AlGaInP system the electron effective mass is rather large, so the width of the miniband is not so large. Therefore the calculated quantised energy gaps will be in good agreement with real ones.

We have calculated the electron wave reflectivities with the various well and barrier combinations whose calculated quantised energy gaps at the MQB region are greater than that of active layer.

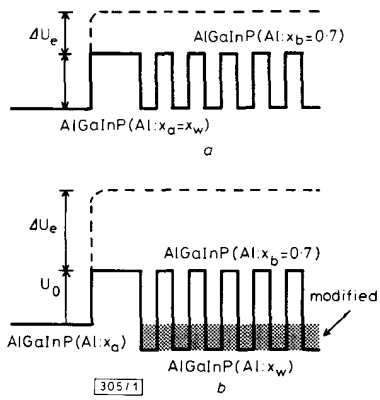

Fig. 1 *Potential energy profiles of MQB*
a Original MQB
b Modified MQB

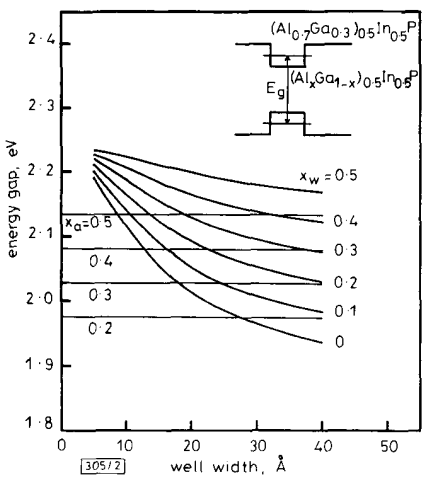

Fig. 2 *Quantised energy gap calculated in simple square well model as function of well width with varying Al fraction of well layer*

Fig. 3 shows the relation between the maximally increased barrier height ΔU_e among the various combinations and the built in potential barrier height U_0 in the original and modified MQB structure. In the original MQB, the maximum ΔU_e values strongly depend on U_0 and increase exponentially with the U_0 value. However, in the modified MQB, we can obtain sufficient ΔU_e of more than 300 meV even for small U_0.

We have also calculated the actual potential barrier height U_a under the biased condition, considering ΔU_e and the variation of Fermi level changes in the MQB region.[4] The actual potential barrier height U_a under biased condition is determined by the energy gap difference ΔE_g between the active and *p*-cladding layer and the Fermi level in the *p*-cladding layer, and its value of conventional DH lasers is expressed as $U_a \simeq \Delta E_g - (E_{fp} - E_v)$, where E_{fp} is the Fermi level of the *p*-cladding layer and E_v is the valence band energy level of the *p*-cladding layer. For an MQB applied laser, its height will be the amount of the above mentioned value and effective potential barrier height ΔU_e increased by MQB, i.e. $U_a \simeq \Delta E_g - (E_{fp} - E_v) + \Delta U_e$. However, if we construct the *p*-doped MQB with thicker well, the Fermi energy of the *p*-cladding layer is located inside the inhibited band compared to that of the bulk cladding layer and this results in a lowering of the actual potential barrier height. The Fermi level is calculated